Optimal selection of distortion model parameters for projection lenses using phasogrammetric self-calibration

Ali Babaei[1]*, Mohammad Saadatseresht[1]

[1] School of Surveying and Geospatial Engineering, College of Engineering, University of Tehran, Tehran, Iran

ABSTRACT

Three-dimensional measurement of coordinates in different optical metrology techniques involves the measurement of image coordinates and/or phase values as observations as well as system parameters. These system parameters are usually determined through a calibration process. Self-calibration of digital fringe projection systems takes advantage of the fringe projection technique in a photogrammetric mathematical model. Many pieces of research have shown the capability of this technique which is called phasogrammetry, to achieve high accuracy and reliability. However, the difference between projection lenses and imaging lenses has not been investigated yet. In this paper, a set of experiments is performed to analyze the behavior of systematic errors in digital projectors as the basic component of this method. The results indicate that the well-known physical model of camera in close range photogrammetry might be used for digital projectors. The best results if the 3D measurement of the test object achieved where the first term of radial distortion K1 and the first in-plane distortion parameter B1 are involved in the self-calibration of the digital fringe projection system.

1. Introduction

The measurement of three-dimensional object coordinates in different optical metrology methods, such as photogrammetry, digital fringe projection, and Moiré techniques, involves the measurement of pixel coordinates or phase in the camera or projector sensor frame, as well as system parameters. These parameters usually describe the optical and geometrical characteristics of the system, such as interior and exterior orientation parameters of camera and projector or relative orientation parameters between camera and projector, and are usually determined before the measurement process in a calibration procedure (Kirschner et al., 1997). In the digital fringe projection technique, system calibration involves determining the phase-to-height mapping using flat plate translation over the measurement volume, which can be time-consuming and requires precise equipment. Alternatively, stereo calibration computes the interior and exterior orientation parameters of the projector-

camera system using a calibration plate placed in several positions and orientations. Only an accurate scale is required to introduce the scale to the measured 3D coordinates, without requiring information about the calibration plate. The homography method was proposed to calibrate projector-camera for a smart presentation system that pre-wraps the images before projection to ensure a perfectly aligned and rectilinear image on the projection screen (Sukthankar et al., 2001). Therefore, the projector can be freely placed anywhere in the room, where it less interferes with the speaker or audience. A steerable projector calibration method based on planar homographies was proposed that treated the projector the same as a camera, to obtain eight intrinsic parameters of the projector; focal length, aspect ratio, two parameters for the principal point, and four parameters for radial and tangential distortion, while assuming zero pixel skew (Ashdown & Sato, 2005). In addition to the mentioned methods, two different techniques

with the photogrammetric point of view were proposed to calibrate a digital projector (Knyaz, 2006). The first method used two calibrated cameras to generate a virtual three-dimensional test field that is used to calibrate the projector, while the second one synthesized the test field images for the projector, then the camera-projector pair was calibrated in a standard bundle adjustment. This method utilized ten additional parameters to describe the projector model; two parameters for the principal point, two-scale factors in x and y directions, an affinity parameter, three radial distortion parameters, and two decentering lens distortion. A method was proposed for the calibration of intrinsic and extrinsic parameters of both camera and projector in a structured light system (Fernandez & Salvi, 2011) based on Zhang's calibration method (2000) implemented in Bouguet's camera calibration toolbox. First, a regular camera calibration process was performed. A planar homography was used to bring 2D coordinates of the projected checkerboard pattern to the reference frame of the camera, then the intrinsic and extrinsic parameters of the projector were computed. Local homographies were also used to estimate the coordinates of the calibration points in the projector image from the points in the calibration object (Moreno et al., 2012). The main contribution was finding the correspondences between the projector and camera pixels that were carried out by projecting a sequence coded targets, like those used in object scanning. A different method was proposed to calibrate a camera and projector that used collinearity equations rather than homography (Portalés et al., 2015). Two image sets of a checkerboard calibration plane were captured in different positions, with and without a projected checkerboard pattern. The camera interior orientation parameters were computed based on Zhang's method using 2D image coordinates of corners and corresponding 3D object coordinates that were easily computed knowing the dimension of the squares on the checkerboard. Then, the exterior orientation parameters of the camera were computed by a spatial resection. In order to calibrate the projector, the same procedure was applied with an additional step to establish 3D coordinates of the projected checkerboard corners. It was fulfilled by inputting camera exterior orientation parameters, 2D coordinates of the corners in the projector image, and knowing the geometry of the calibration object which was a plane here with Z=0 to the rearranged collinearity equations. While the proposed method allows estimating interior and exterior orientation parameters separately, the accuracy of the projector calibration depends on the accuracy of the camera calibration. Liu et al. (2017) used a bundle adjustment strategy to optimally locate the coordinates of feature points on the planar reference target, allowing compensation for the fabrication errors. A method was proposed in (Zhang et al., 2017) to determine the projector pixel coordinates of the marker points of a calibration target accurately in terms of projective transform. With the method, the projector can be calibrated with an accuracy of the sub-pixel level. The method is applicable to the calibration target with a chessboard pattern or a circle pattern, and the calibration result is independent of the results of camera calibration. However, this method requires repetitive changing of the target board with a white plate and acquiring data. Moreover, it is based on Zhang's calibration technique which does not involve high-accuracy physical model parameters to describe lens distortions. A multi-view calibration and 3D measurement method was proposed based on digital fringe projection method (Gai et al., 2019) by which digital fringe projection and a phase map are used to establish global calibration information. Large-sized calibration targets and other auxiliary calibration devices are not required when using this method. However, this method still requires extensive projection and capturing of fringe patterns. In (Chen et al., 2020), the fundamental assumption is that the existing calibration methods are subjected to the low accuracy because planar boards with a checker, ring or dot are used to provide only limited number (tens to hundreds) of reference points with lower accuracy (pixel level). Therefore, a calibration method was proposed using a liquid crystal display (LCD) screen to offer high-density reference points. The experimental results demonstrated that the proposed 3D calibration method achieved the higher measurement accuracy of the shape data compared with the existing state of the art methods. However, the method was only compared with Zhang's method, which is not capable of modeling accurate lens distortions. The drawback of all the methods mentioned above is the dependency of the projector calibration result to the camera calibration procedure. All of the camera-projector calibration methods that were reviewed before, more and less, use the same concept: they perform projector calibration using a virtual reference, which has been established by a photogrammetric measurement process utilizing camera observations. So, every amount of error in the camera calibration process, and the computation of reference frame coordinates, directly conveys to the projector calibration procedure as it takes those as inputs. Unlike these techniques, the self-calibration of the projector (phasogrammetry technique) does not rely on the computed virtual reference points. It directly determines the system parameters along with 3D coordinates of the measured object from the first observations: phase values. Moreover, the standard procedure of calibration requires several camera-projector setups, projecting and capturing several dozens of binary and phase-shifted fringe patterns. The difference between our method and other reviewed techniques is that they need calibration before measurement, while our method is a self-calibration procedure, which does not involve performing a calibration before measurement. All the required parameters of the system are computed simultaneously with 3D object coordinates. Thus, it is safe to say that data acquisition and

the processing time is shorter than other methods. The collinearity equations that are the basis of the analytical photogrammetry describe the relationship between object point, its corresponding image point, and the perspective center of the camera. These equations can be solved for both unknown object coordinates and system parameters simultaneously, which is called self-calibration. This technique does not require any prior information about the system parameters. The method does not require prior calibration and target on the object surface, provides redundant observations that increase the reliability of the calculated coordinates, and bypasses the time-consuming and complicated process of finding corresponding points (matching). It is also immune to the temporal instabilities in the system and environment (Kirschner et al., 1997) (Schreiber & Notni, 2000). The same concept was adopted for the fringe projection technique in combination with photogrammetry, which resulted in a self-calibration fringe projection technique (Bräuer-Burchardt et al., 2014). Although the proposed self-calibration of the digital fringe projection system employs common photogrammetric additional parameters for describing the deviation of coordinates from the strict central projection, it does not take into account the structural difference of imaging lens of camera and projection lens of the projection device.

This work presents an analysis of the self-calibration digital fringe projection system, focusing on the additional parameters describing the systematic error of the projector lens. Previous works such as (Kirschner et al., 1997) utilized the same additional parameters of the imaging lens for the projector, while did not provide further analysis. The physical radial distortion model with three terms (K1, K2, and K3) was used to correct the projector distortions (Schreiber & Notni, 2000). The main drawback of these works was that the same behavior was assumed for imaging lens and projection lens and the difference between the camera lens and projection lens was not taken into account. Although the collinearity condition applies to both cameras and projectors, they are designed and built based on different concepts and functionality. In this paper, the well-known physical additional parameters model, which is often used in close-range photogrammetry camera calibration, is adapted for digital projector self-calibration. The self-calibration of the digital fringe projection system involves a fixed camera compared to the object space and a digital projector that projects two sets of fringe patterns, horizontal and vertical, onto the object's surface from different positions. A modified collinearity equation describes the relationship between image space and object space. A well-known physical model that is capable of modeling symmetric radial distortion, decentering distortion, image plane unflatness is utilized to model the distortions of the optical component of the projector.

The rest of this paper is organized as follows: The next section presents the mathematical model of the self-calibration of digital fringe projection systems. A well-known additional parameter model for the camera lens is expressed, then optics of the projection lens is discussed in detail and compared to that of the general imaging lens. Section 3 provides experiments and test results. The results of the experiments are discussed in Section 4. Finally, Section 5 concludes the paper.

2. Mathematical Model of Self Calibration Digital Fringe Projection System

The self-calibration of the digital fringe projection system involves a fixed camera with respect to the object space and a digital projector that projects two sets of fringe patterns, horizontal and vertical, onto the object's surface from different positions. The configuration of this system is illustrated in Figure 1. Two positions are the minimum requirement, while more positions increase the reliability of the measurements.

A vertical and a horizontal phase map are computed for each projector position using captured images. These phase values are the replacements of image coordinates in the collinearity equations, as they indicate the position of the point in the projector sensor. The modified collinearity equation (Schreiber & Notni, 2000) is given by:

$$
\xi_{i,j}^k - \xi_0^k + d\xi_{i,j}^k =
$$
$$
(\frac{2\pi}{\lambda} C_k) \frac{r_{11}^k(X_m - X_0^k) + r_{21}^k(Y_m - Y_0^k) + r_{31}^k(Z_m - Z_0^k)}{r_{13}^k(X_m - X_0^k) + r_{23}^k(Y_m - Y_0^k) + r_{33}^k(Z_m - Z_0^k)},
$$
$$
\eta_{i,j}^k - \eta_0^k + d\eta_{i,j}^k =
$$
$$
(\frac{2\pi}{\lambda} C_k) \frac{r_{12}^k(X_m - X_0^k) + r_{22}^k(Y_m - Y_0^k) + r_{32}^k(Z_m - Z_0^k)}{r_{13}^k(X_m - X_0^k) + r_{23}^k(Y_m - Y_0^k) + r_{33}^k(Z_m - Z_0^k)}.
$$

(1)

In this relationship $\xi_{i\,j}^k$ and $\eta_{i\,j}^k$ denotes the vertical and horizontal phase value of the kth position of the projector at the camera pixel (i,j) and $[X_m, Y_m, Z_m]$ are the corresponding object coordinates for that pixel. Similarly, ξ_0^k and η_0^k are the phase values at the principal point of the projector at the kth position. The $d\xi_{i,j}^k$ and $d\eta_{i\,j}^k$ are the correction terms that contain additional parameters and will be discussed later. The C_k, $[r_{1,1}, r_{1,2}, r_{1,3}, r_{2,1}, r_{2,2}, r_{2,3}, r_{3,1}, r_{3,2}, r_{3,3}]_k$, and $[X_0, Y_0, Z_0]_k$ are the principal distance of the projector, the elements of the rotation matrix of the projector, and the coordinates of the perspective center of the projector at the kth position. The formulation above fully describes the parameters of the projector(s). It also allows calculating the 3D object coordinates and calibrating the parameters simultaneously.
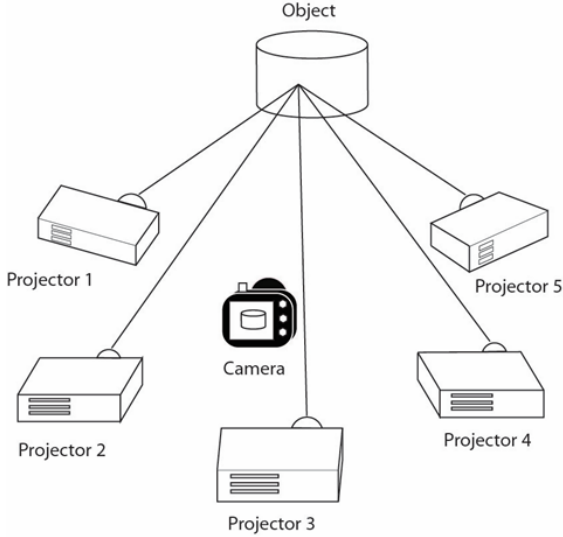
Figure 1. Schematic of digital fringe projection self-calibration

2.1. Physical model for camera calibration

A well known physical model capable of modeling symmetric radial distortion, decentering distortion, image plane unflatness, and In-plane image distortion was proposed by Fraser (1997) for self-calibration of cameras in close-range photogrammetry. This model is the basis of this work as stated in equation 2:

$$\Delta x = \Delta x_{radial} + \Delta x_{decentering} + \Delta x_{in-plane} + \Delta x_{out-of-plane},$$
$$\Delta y = \Delta y_{radial} + \Delta y_{decentering} + \Delta y_{in-plane} + \Delta y_{out-of-plane}. \quad (2)$$

The terms Δx_{radial} and Δy_{radial} corrections for symmetric radial distortion. The radial distortion which is symmetric compared to the principal point, represented by an ideally infinite odd ordered polynomial series, as a consequence of the nature of Seidel aberrations (Fraser, 1997):

$$\Delta r = K_1 r^3 + K_2 r^5 + K_3 r^7, \quad (3)$$

where K_i terms represent the radial distortion coefficients, and r is the radial distance from the principal point. The corrections for x, y image coordinates are computed from:

$$x'_r = \bar{x}' \, r / r,$$
$$y'_r = \bar{y}' \, r / r. \quad (4)$$

where $\bar{x} = x - x_0$ and $\bar{y} = y - y_0$.

The imperfection in aligning optical elements of a lens in the same optical axis causes both radial and tangential image distortion, which is known as decentering distortion. It can be corrected by the model proposed by Brown (1971):

$$x'_{decentering} = [P_1(r^2 + 2\bar{x}^2) + 2P_2\bar{x}\bar{y}][1 + P_3 r^2 + ...],$$
$$y'_{decentering} = [2P_1\bar{x}\bar{y} + P_2(r^2 + 2\bar{y}^2)][1 + P_3 r^2 + ...]. \quad (5)$$

where P_1, P_2, P_3 are coefficients of decentering distortion. The focal plane unflatness introduces an error into the image coordinate in high accuracy photogrammetric applications. Usually, in metric analogue cameras, the topography of the image plane is measured directly and the derived image coordinate perturbation is modeled by a third-order or fourth-order polynomial equation:

$$\begin{Bmatrix} \Delta x_{out-of-plane} \\ \Delta y_{out-of-plane} \end{Bmatrix} = \begin{Bmatrix} \bar{x}/r \\ \bar{y}/r \end{Bmatrix} \sum_{i=0}^{n} \sum_{j=0}^{i} a_{i,j} \bar{x}^{(i-j)} \bar{y}^j. \quad (6)$$

However, the applicability of these methods to CCD sensors is uncertain. It is reported that at an incidence angle of 45 degrees, a 10-micron departure from planarity produces an image displacement of the same magnitude (Fraser, 1997). The in-plane distortion correction model is a two-term model for correcting x-coordinate. The B1 term accounts for different scales in x- and y- pixel spacing (affinity term), and B2 accounts for non-orthogonality between x and y axes (shear term):

$$\Delta x_{in-plane} = B_1\bar{x} + B_2\bar{y},$$
$$\Delta y_{in-plane} = 0. \quad (7)$$

while the in-plane error was significant in analogue photogrammetry, modern digital sensors are not affected by this error. "The problems of physical in-plane distortion that adversely influenced film-based photogrammetry are fortunately absent from digital systems employing high resolution, large-area CCD cameras. The geometric integrity of the layout of the pixel array is typically precise to the 0.1μm level." (Fraser, 1997).

2.2. Optics of Digital Projectors

The optics of a digital projector can be simplified into two main parts: the optical illumination system (also known as condenser lens system) that provides uniform illumination on the sensor and the projection lens that projects the enlarged image onto a screen (Brennesholtz & Stupp. 2007). The quality of the projected image is defined by its optical characteristics, such as system magnification, the size of the projection beam, and the energy distribution of the projected image (Chang & Shieh, 2000). Most of the normal projection lenses share some main features: wide field of view (usually 80 to 120 degree), larger relative aperture, small system axis aberration, and minimum distortion (Chang & Shieh, 2000). In recent years and with the advancement of the Digital Micromirror Device (DMD) technology, the focus of optical designers has been shifted toward designing miniaturized and lightweight projection systems. The traditional telecentric projection lens now is going to be replaced by non-telecentric lenses which offer almost the same quality while lowering the size and weight of the system as well as the cost of manufacturing (Sun, W.-S., et al.,2011; Sun, W.-s. and J.-W. Pan, 2017). However, the design criteria are

almost the same. These projection optic system features must be considered in the calibration process, where additional parameters are used to describe the lens system behavior.

The projection lenses are designed to minimize the distortions, usually set a goal of 1% maximum distortion (TI Application Note, 2017). In order to reach this goal, aspheric lenses are implemented in projection lens systems. The surfaces profile of an aspheric lens is neither a portion of a sphere nor of a circular cylinder. An aspheric lens has a more complex surface compared to a simple lens. This characteristic eliminates spherical aberration and reduces other optical aberrations. Hence, using a sphere enhances image quality, minimizes distortion, reduces distortions at wide angels, and also improves corner resolution of the system (Pruss et al., 2008). By addressing the structure of projection lenses, it seems the physical model of imaging lenses can be used to model systematic errors of projection lenses with some considerations. Some tests are designed, implemented and analyzed to study these considerations in the next section.

3. Experiments and Results

The experimental setup consists of a camera with 1024×1024 resolution and an off-the-shelf pico DLP projector with 858×480 native resolution. The camera was fixed during the measurement while the projector was moved to nine different positions to illuminate fringe patterns onto the object's surface. Based on a given set of user accuracy requirements, the network must be designed, diagnosed, and, if necessary, optimized. The problem of optimal design can be classified into four interconnected problems: zero-order design embraces the datum problem, first-order design of the configuration problem, second-order design of the weight problem, and third-order design of the densification problem (Fraser, 1984). The principle of network design was considered to provide an optimum network geometry. A double hemisphere object with known dimensions was measured by a digital fringe projection self-calibration method for numerical analysis. Figure 2 illustrates the projector positions and the point cloud of the test object.

In the self-calibration of digital fringe projection systems, the optical and geometrical attributes of the camera are not involved in the calculations. The camera records the projected patterns that are used for phase calculation. For each pixel in the camera, eventually, a 3D object coordinate is calculated, where the number of observations is equal to the number of valid pixels in the camera image. The valid pixels are those pixels that are illuminated by the projector from at least two different positions. The resolution of the measurement, therefore, depends on the resolution of the camera. The valid pixels are demonstrated as a visibility map in Figure 3.
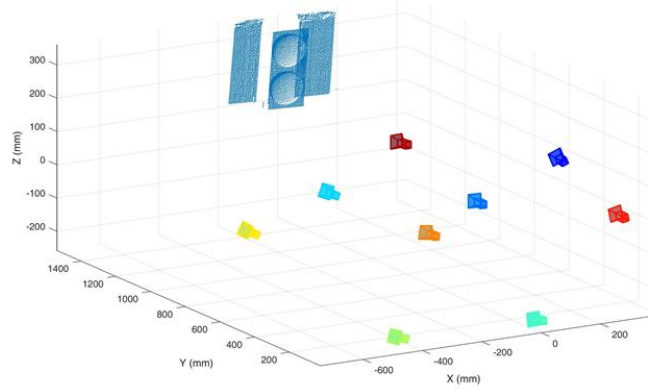

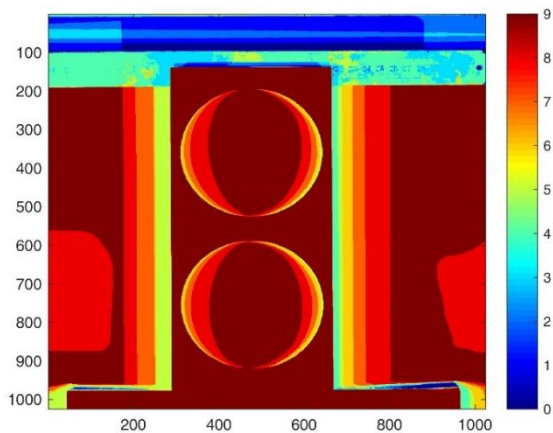Figure 2. Configuration of the projectors and point cloud of the test object.

Figure 3. Visibility map of the test objects shows the number of projectors illuminating each camera pixel.

The observations are usually highly redundant in the self calibration of digital fringe projection systems, and all the observations are not required to determine system parameters. Therefore, the processing procedure was divided into two steps to avoid unnecessary computations and speed up the process. In the first step, self calibration was performed using some sampled points which were well-distributed over the scene. Then, 3D coordinate calculation of all valid pixels was done with the computed parameters in the previous step.

A set of experiments are designed, performed, and analyzed to investigate how the additional parameters should be used in digital projector self calibration. It is assumed that the interior orientation parameters of a digital projector are constant and have not been changed during the measurements. In the first experiment, all additional parameters, i.e., $K_1, K_2, K_3, B_1, B_2, P_1, P_2$, are involved in the self calibration process. This test provides an overall estimate of the behavior of the projection lens system, as well as the correlations between additional determined parameters. In the second test, in-plane distortion correction

terms, B_1 and B_2, are ignored and self-calibration is performed with radial and decentering distortion correction terms to determine the influence of in-plane distortion correction on the 3D measurement result. Although the decentering parameters are necessary to describe the probable misalignment of optical competent in the projection lens, they were ignored in the third test because a high correlation between decentering distortion parameters and principal point components are expected (Brown, 1971). In the fourth test, the shear term, B_2, was ignored because it had been shown (Brown, 1971) that B2 was invariably insignificant. In order to study the total impact of decentering distortion and in-plane distortion correction terms on the self-calibration process, the final test carried out only involving the radial distortion correction. The determined parameters of the projector in all tests are summarized in Table 1.

Table 1. Additional Parameters (A.P.s) Model in all tests; Test I: radial, decentering, and in-plane distortion terms; Test II: the first term of radial and decentering distortion terms; Test III: the first term of radial and in-plane distortion terms; Test IV: the first terms of radial distortion and in-plane distortion; and Test V: only the first term of radial distortion are involved in the self-calibration process.

Parameter	Test I Value	Test I Std.	Test II Value	Test II Std.	Test III Value	Test III Std.	Test IV Value	Test IV Std.	Test V Value	Test V Std.
f	8.9353	6.13e-02	8.9272	6.01e-02	8.9391	6.10e-02	8.9255	6.00e-02	8.9307	5.93e-02
xp	-0.0263	9.43e-02	-0.0613	8.22e-02	-0.0802	3.06e-02	-0.0406	1.83e-02	-0.0423	1.84e-02
yp	-1.3056	8.76e-02	-1.2908	7.54e-02	-1.2406	4.56e-02	-1.2258	4.42e-02	-1.2045	3.17e-02
K1	-1.122e-03	6.68e-04	8.49e-04	1.56e-04	9.17e-04	1.58e-04	9.09e-04	1.59e-04	8.88e-04	1.54e-04
K2	5.184e-04	1.63e-04	0	0	0	0	0	0	0	0
K3	-4.210e-05	1.34e-05	0	0	0	0	0	0	0	0
P1	-1.159e-04	3.97e-04	4.56e-05	2.83e-04	0	0	0	0	0	0
P2	3.491e-04	4.96e-04	2.47e-04	2.71e-04	0	0	0	0	0	0
B1	2.777e-04	1.15e-03	0	0	-3.01e-04	6.13e-04	-3.19e-04	6.07e-04	0	0
B2	5.873e-04	8.76e-04	0	0	7.08e-04	5.90e-04	0	0	0	0

Table 2. The estimated radius of hemisphere and RMSE of fit for the implemented tests.

Test	Radius Difference Hemisphere 1	Radius Difference Hemisphere 2	Radius Difference Mean	RMSE of Fit Hemisphere 1	RMSE of Fit Hemisphere 2	RMSE of Fit Mean
Test I: All A.P.s	0.103 mm	0.381 mm	0.242 mm	0.259 mm	0.391 mm	0.325 mm
Test II: K1, P1, P2	0.167 mm	0.346 mm	0.257 mm	0.242 mm	0.401 mm	0.322 mm
Test III: K1, B1, B2	0.110 mm	0.368 mm	0.239 mm	0.365 mm	0.246 mm	0.306 mm
Test IV: K1, B1	0.128 mm	0.051 mm	0.090 mm	0.239 mm	0.364 mm	0.302 mm
Test V: K1	0.308 mm	1.003 mm	0.656 mm	0.338 mm	0.320 mm	0.329 mm

Table 3. The correlation between additional parameters in Test I, where all radial, decentering, and in-plane distortion parameters are involved in the self-calibration process.

	C	xp	yp	K1	K2	K3	P1	P2	B1	B2
C	1	-0.05	0.029	-0.065	-0.017	0.039	0.013	0.028	0.094	0.087
xp		1	-0.179	0.002	-0.075	0.078	**-0.943**	0.263	0.230	**0.405**
yp			1	0.061	0.032	-0.038	0.181	**-0.844**	**-0.505**	0.052
K1				1	**-0.909**	**0.840**	-0.085	-0.198	-0.117	0.224
K2					1	**-0.982**	0.127	-0.043	-0.099	-0.151
K3						1	-0.114	0.067	0.102	0.114
P1							1	-0.216	-0.209	**-0.648**
P2								1	**0.830**	-0.155
B1									1	-0.101
B2										1

Table 4. The correlation between additional parameters in Test III, where only the first radial distortion term and in-plane distortion parameters are involved in the self-calibration process.

	C	xp	yp	K1	K2	K3	P1	P2	B1	B2
C	1	-0.156	0.089	-0.190	0	0	0	0	0.151	0.164
xp		1	0.256	-0.162	0	0	0	0	-0.073	**-0.800**
yp			1	**-0.726**	0	0	0	0	**0.675**	-0.237
K1				1	0	0	0	0	-0.255	0.071
K2					1	0	0	0	0	0
K3						1	0	0	0	0
P1							1	0	0	0
P2								1	0	0
B1									1	-0.015
B2										1

The exterior orientation parameters of the projectors that are determined simultaneously during the self-calibration procedure were used for dense object reconstruction in a multi-ray intersection procedure. Table 2 demonstrates the results of the performed tests. The radius of the test object hemisphere was 50.80 mm, and the mean fitted radius and mean RMSE of fit to the measured point cloud in Test I, Test II, Test III, Test IV, and Test V were 50.558 mm and 0.325 mm, 50.544 mm and 0.322 mm, 50.561 mm and 0.306 mm, 50.711 mm and 0.302 mm, and 50.145 mm and 0.329 mm, respectively. The point cloud of the measured object and the meshed surface are presented in Figure 4. The best result, i.e., both the smallest standard deviation and fitting residual, were achieved in Test IV where only the first terms of radial distortion and in-plane distortion parameters were involved in the self-calibration process.

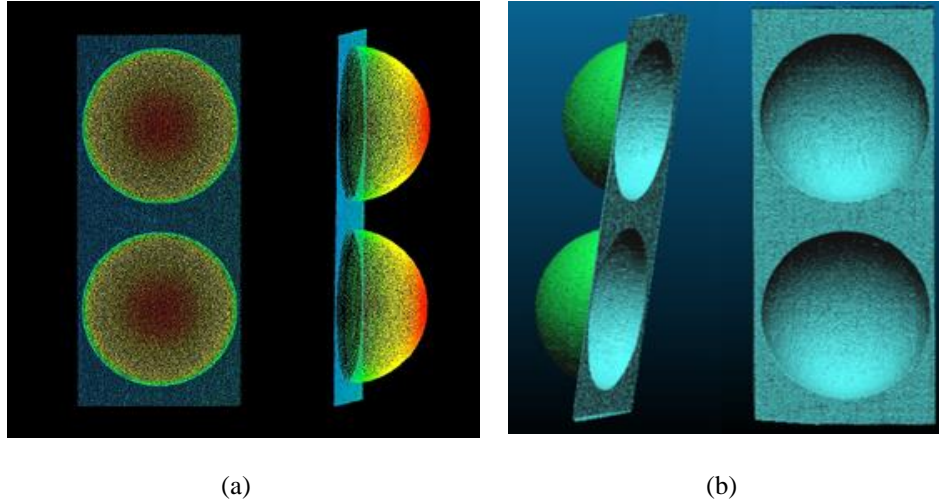(a)   (b)

Figure 4. 3D reconstruction of the test object: (a) Point cloud; (b) Meshed point cloud.

Table 5. The correlation between additional parameters in Test IV, where only the first radial distortion term and the first in-plane distortion term are involved in the self-calibration process.

	C	xp	yp	K1	K2	K3	P1	P2	B1	B2
C	1	-0.029	0.129	-0.201	0	0	0	0	0.151	0
xp		1	0.098	-0.123	0	0	0	0	-0.118	0
yp			1	**-0.728**	0	0	0	0	**0.694**	0
K1				1	0	0	0	0	-0.257	0
K2					1	0	0	0	0	0
K3						1	0	0	0	0
P1							1	0	0	0
P2								1	0	0
B1									1	0
B2										1

4. Discussion

A projector can be treated as an inverse camera. Therefore, the same concept and physical model can be adapted to model a projection lens. Many works in the literature have discussed the physical model of the camera lens (Fraser, 2001; Remondino & Fraser, 2006). The 10-parameter physical model is efficient, robust, and enabling calibration of a wide variety of different lenses. However, the main drawback of this model is the high correlation between different parameters. The high correlation between two parameters indicates that the error caused by one parameter can be partially corrected by the other. There are two types of correlations; correlations between interior orientation parameters and exterior orientation parameters, and correlations between interior orientation parameters itself. In the first type of correlations, a strong geometry of camera/projector configuration diminishes these correlations. The second type of correlation is of major concern in self-calibration practice and should be handled carefully.

In this study, the principal of the camera (here projector) network design is applied, so the first type of correlations is negligible. The correlations between the determined interior orientation parameters in Test I are provided in Table 3. It has been demonstrated that for the majority of medium-angle, non-photogrammetric lenses employed in today's metric and nonmetric close-range cameras, the third-order term is sufficient to account for the induced aberrations (Fraser, 2001). For wide-angle lenses, higher-order terms (very rarely above seventh order) are often required to adequately model lens distortion. For low to medium accuracy CCD camera applications, the use of the K_1 term alone will usually suffice since the most commonly encountered distortion profile is that of the third-order barrel distortion. The inclusion of K_2 and K_3 might be warranted for higher accuracy applications. The distortion coefficients

K_1, K_2 and K_3 are generally highly correlated, usually indicating that most of the error signal is accounted for by the cubic term K_1r^3. This coupling is restricted to the radial distortion parameters and is of little importance as far as the overall numerical stability of the self-calibration adjustment is concerned. Here, high correlations exist between radial distortion parameters, 91% between K_1 and K_2, 85% between K_1 and K_3, and 98% between K_2 and K_3. It means that using only K_1 can sufficiently correct the radial distortion effect. In the next experiments, Test II, Test III, Test IV, and Test V only K1 term is involved in correcting the radial distortion effect. The self-calibration was repeated without in-plane distortion correction terms in Test II to determine the effect of in-plane correction terms on the result. The next significant correlations are correlations between the principal point offset and the decentering distortion parameters. The 94% correlation between x_p and P_1, and 84% between y_p and P_2 suggest that decentering distortion parameters can be removed from additional parameters' model with no adverse effect on the self-calibration result as showed in Test III. The in-plane correction terms, B_1 and B_2, are also correlated with the principal point offset, but not as high as decentering distortion parameters. The correlations between in-plane parameters in Test III have changed significantly as shown in Table 4. Removing the decentering parameters from the self-calibration process increased correlations between x_p and B_2 and between y_p and B_1. As discussed earlier, the shear parameter effect is insignificant, so B_2 was removed in Test IV and the correlations are shown in Table 5. Finally, Test V was performed with only the first term of the radial distortion term.
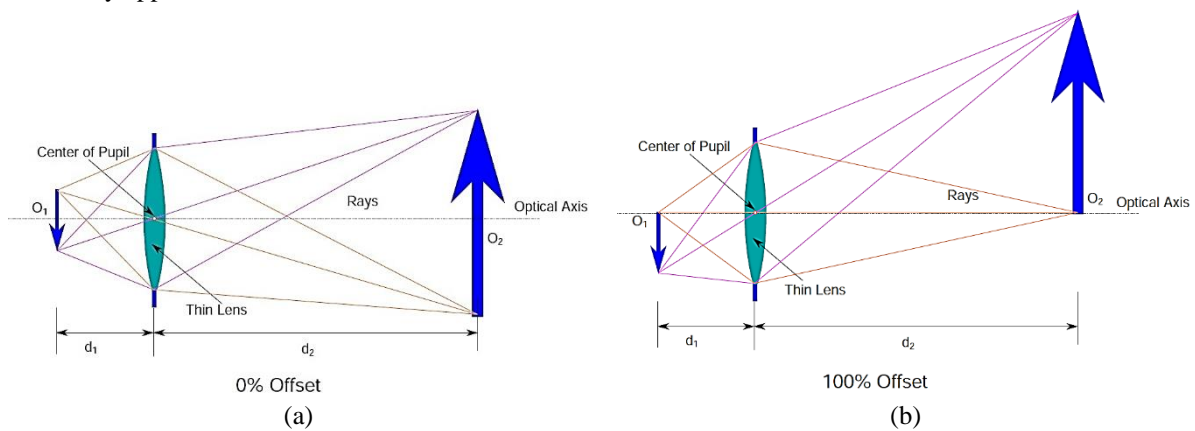

Figure 5. Schematic illustration of the projector offset: (a) 0% offset; (b) 100% offset.

The results of 3D reconstruction that are summarized in Table 2 show that, as predicted before, removing the decentering correction terms does not decrease the accuracy, while ignoring the in-plane distortion parameters despite their correlations with principal point offset, degrades the result of 3D reconstruction. The probable non-perpendicularity of the optical axis to the projector sensor surface produces an affine distortion in the projected image. Therefore, the in-plane distortion correction should be involved in the self-calibration process. Despite the high correlation between B1 and y_p in Test IV, ignoring B_1 and performing self-calibration without both decentering and in-

plane distortion parameters have resulted in the worst accuracy in Test V.

According to the experiments, the proper additional parameters model that describes the projection lens used in this experiment seems to involve both the first terms of radial distortion and in-plane distortion correction as stated in equation 8:

$$\Delta\xi = \Delta\xi_{\text{radial}} + \Delta\xi_{\text{in-plane}},$$
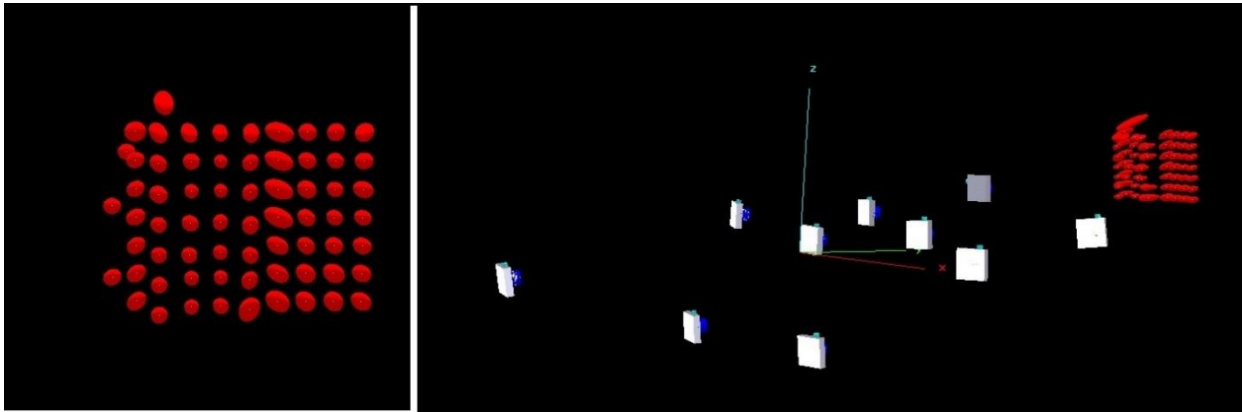$$\Delta\eta = \Delta\eta_{\text{radial}} + \Delta\eta_{\text{in-plane}}. \tag{8}$$

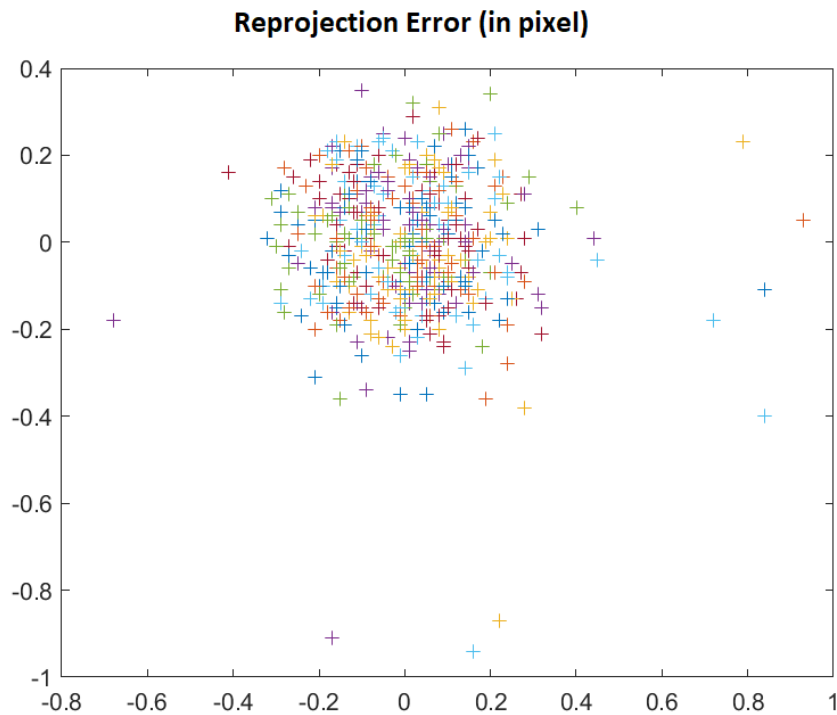Figure 6. Error Ellipsoids in Test IV.

Figure 7. Reprojection Error (in pixel) in Test IV.

The unusual large value of term y_p in Table 1, is explained by the projector offset. In a DLP projector, offset is a

measure of the shift of the DMD sensor with respect to the optical axis of the projection lens, as shown in Figure 5. In a

0% offset design, the center of the DMD sensor is aligned exactly with the optical axis of the projection lens while in a 100% offset, the DMD sensor is dropped until its upper edge is aligned with the optical axis of the projection lens. This means that if the projector is sitting on a table, in case of 0% offset, the image is projected equally up and equally down from the optical axis, contrary to 100% offset, for which the bottom half of the projected image is blocked, and only the top half of the image reaches the screen. In order to consider the offset of the projector, the y component of the principal point is set to a constant value, which is the product of half of DMD width and DMD pixel size. Figure 6 illustrates the error ellipsoid of object points in the self-calibration of the projector. As expected, the semi-major axis of the ellipsoid is parallel to the depth of the object, here y axis. The reprojection errors of test IV are shown in Figure 7. The selected terms sufficiently described the distortions in the projector lens. Regardless of some blunders, most of the reprojection errors distributed around zero.

5. Conclusions

This work presented an analysis of additional parameters in the self-calibration of digital fringe projection systems. The well-known physical model of cameras can be used for projectors with some considerations. A strong network geometry configuration can alleviate the correlations between the interior orientation parameters and the exterior orientation parameters. The analysis of correlations between different interior orientation parameters showed that the first term of radial distortion K_1, and the first term of in-plane distortion B_1 could sufficiently describe the systematic error behavior of projection lenses and generate the most accurate and reliable 3D measurement.

References

Kirschner, V.; Schreiber, W.; Kowarschik, R.M.; Notni, G. (1997) 'Self-calibrating shape-measuring system based on fringe projection' In *Lasers and Optics in Manufacturing III*, International Society for Optics and Photonics.

Sukthankar, R.; Stockton, R.G.; Mullin, M.D. (2001) 'Smarter presentations: Exploiting homography in camera-projector systems' In *Eighth IEEE International Conference on Computer Vision, ICCV 2001*, IEEE.

Ashdown, M.; Sato, Y. (2005) 'Steerable Projector Calibration' In *IEEE Computer Society Conference on Computer Vision and Pattern Recognition, CVPR 2005*, IEEE.

Knyaz, V. (2006) 'Automated Calibration Technique for Photogrammetric System based on a multi-media projector and a CCD Camera' In *Comission V Symposium of ISPRS* , Dresden. ISPRS.

Fernandez, S.; Salvi, J. (2011) 'Planar-based camera-projector calibration' In *Image and Signal Processing and Analysis (ISPA),* IEEE.

Zhang, Z. (2000) 'A flexible new technique for camera calibration' *IEEE Trans. Pattern Anal. Mach. Intell.*, 22(11), 1330-1334.

Camera Calibration Toolbox for Matlab. Available online: http:// www.vision.caltech.edu /bouguetj/ calib_doc/ .

Moreno, D.; Taubin, G. (2012) 'Simple, accurate, and robust projector-camera calibration' In *Second International Conference on 3D Imaging, Modeling, Processing, Visualization & Transmission*, IEEE.

Portalés, C.; Ribes- Gómez, E.; Pastor, B.; Gutiérrez, (2015) 'A. Calibration of a camera–projector monochromatic system' *Photogramm. Rec.*, 30(149), 82-99.

Bräuer-Burchardt, C.; Breitbarth, A.; Kühmstedt, P.; Notni, G. (2014) 'High-speed three-dimensional measurements with a fringe projection-based optical sensor' *Opt. Eng.*, 53(11), 112213-112213.

Schreiber, W.; Notni, G. (2000) 'Theory and arrangements of self-calibrating whole-body three-dimensional measurement systems using fringe projection technique', *Opt. Eng.*, 39(1), 159-169.

Fraser, C. S. (1997) 'Digital camera self-calibration', *ISPRS J. Photogramm. Remote. Sens.*, 52(4), 149-159.

Duane, C. B. (1971) 'Close-range camera calibration' *Photogramm. Eng.*, 37, 855-866.

Brennesholtz, M. S.; Stupp, E. H. (2007) 'Introduction in Projection Displays' 2nd. Ed.; John Wiley & Sons: Chichester, UK, 9780470770894.

Chang, C.; Shieh, H.D. (2000) 'Design of illumination and projection optics for projectors with single digital micromirror devices' *Appl. Opt.*, 39, 3202-3208

Texas Instruments. DLP System Optics Application Note. Available online: http://www.ti.com (accessed on 7 December 2017)

Pruss, C.; Garbusi, E.; Osten, W. (2008) 'Testing Aspheres' *Opt. Photon. News.*, 19(4), 24-29.

Sun, W.-S., et al. (2011) 'Optical design for the DLP pocket projector using LED light source' *Physics Procedia 19*: 301-307

Sun, W.-s. and J.-W. Pan (2017) 'Non-telecentric projection lens design for an LED projector' *Applied Optics* 56(3): 712-720

Fraser, C. S. (2001) 'Photogrammetric camera component calibration: A review of analytical techniques' *Calibration and Orientation of cameras in Computer Vision*, Springer: 95-121.

Remondino, F. and C. Fraser (2006) 'Digital camera calibration methods. Considerations and comparisons' *ISPRS Commission V Symposium* 'Image Engineering and Vision Metrology', Dresden, Germany, September 25-27

Fraser, C. S., (1984) 'Network design considerations for non-topographic photogrammetry' *Photogrammetric Engineering and Remote Sensing* 50(8): 1115-1126.

Liu, X., et al. (2017) 'Calibration of fringe projection profilometry using an inaccurate 2D reference target' *Optics and lasers in engineering* 89: 131-137

Zhang, W., et al. (2017) 'Sub-pixel projector calibration method for fringe projection profilometry' *Optics Express* 25(16): 19158-19169.

Gai, S., et al. (2019) 'A flexible multi-view calibration and 3D measurement method based on digital fringe projection' *Measurement Science and Technology* 30(2): 025203.

Chen, C., et al. (2020) 'High accuracy 3D calibration method of phase calculation-based fringe projection system by using LCD screen considering refraction error' *Optics and lasers in engineering* 126: 105870.